Traction and nonequilibrium phase behavior of confined sheared liquids at high pressure

Chiara Gattinoni,[1,*] David M. Heyes,[1,†] Christian D. Lorenz,[2,‡] and Daniele Dini[1,§]
[1]*Department of Mechanical Engineering, Imperial College London, Exhibition Road, South Kensington, London SW7 2AZ, United Kingdom*
[2]*Department of Physics, King's College London, Strand, London WC2R 2LS, United Kingdom*
(Received 15 July 2013; published 13 November 2013)

Nonequilibrium molecular dynamics simulations of confined model liquids under pressure and sheared by the relative sliding of the boundary walls have been carried out. The relationship between the time-dependent traction coefficient, $\mu(t)$, and the state of internal structure of the film is followed from commencement of shear for various control parameters, such as applied load, global shear rate, and solid-liquid atom interaction parameters. Phase diagrams, velocity and temperature profiles, and traction coefficient diagrams are analyzed for pure Lennard-Jones (LJ) liquids and a binary LJ mixture. A single component LJ liquid is found to form semicrystalline arrangements with high-traction coefficients, and stick-slip behavior is observed for high pressures and low-shear velocities, which is shown to involve periodic deformation and stress release of the wall atoms and slip in the solid-liquid boundary region. A binary mixture, which discourages crystallization, gives a more classical tribological response with the larger atoms preferentially adsorbing commensurate with the wall. The results obtained are analyzed in the context of tribology: the binary mixture behaves like a typical lubricant, whereas the monatomic system behaves like a traction fluid. It is discussed how this type of simulation can give insights on the tribological behavior of realistic systems.

DOI: 10.1103/PhysRevE.88.052406 PACS number(s): 68.15.+e, 68.08.−p

I. INTRODUCTION

The tribological properties of confined liquid films are important in a number of engineering applications, for example, in elastohydrodynamic lubrication (EHL), where a lubricant is sheared at high pressure between two bodies in contact. Pressure has the effect of increasing the real contact area between the asperity landscape of the two surfaces [1], as well as changing the rheology of the confined lubricant, so its separate effects are difficult to resolve directly from experiment. In the so-called boundary lubrication regime, the lubricant film may only be a few molecules thick, and a continuum description of the lubricant breaks down. The necessity to consider the molecular discreteness of the lubricant may make rheological constitutive equations developed in other fields, such as for granular systems [2], more applicable. In this work, our attention is mainly directed toward the effects of pressure on the rheology of different types of confined lubricants and their dynamical coupling with the boundary walls. This is also the first step toward the establishment of a direct link between NEMD simulations and the evolution of rheological properties to be passed to macroscopic models developed to study lubrication using the continuum approximation [3].

Confined liquids that are a few molecules thick are known to behave quite differently to bulk liquids at the same temperature and pressure. They have a different phase diagram from the bulk [4,5]. Liquid molecules tend to layer (even order) against a wall and for long and flat-shaped molecules, align parallel to the wall [6–9]. The dynamics of the molecules and the transport behavior also reflect this structural anisotropy. Spatial and temporal intermittency in diffusional processes have been observed in bulk supercooled liquids [10], and the same trends are accentuated in confined liquids, which have a tendency to become more viscous or even "glassy" in comparison to their bulk counterparts [11–13]. Sliding of the two walls, at relatively low apparent or global shear rates, gives rise to so-called "stick-slip" behavior, which has been attributed to cyclical solidification and melting of the confined liquid [14,15], system solidification [16], or structural jamming and orientation [17]. The "yield" stress, the shear stress at the top of the stick region, σ_{xy}, increases with normal pressure, P, according to $\sigma_{xy} = \sigma_{0,xy} + AP$, where $\sigma_{0,xy}$ and A are system-specific constants [18].

Nonequilibrium molecular dynamics (NEMD) computer simulations have proved an invaluable tool with which to investigate sheared molecularly thin confined liquid films. The advantage of NEMD is that the tribological behavior and liquid-wall boundary conditions emerge naturally from the simulation, rather than being introduced in an *ad hoc* way in the model. Although the models presented in this paper are quite simple compared with many experimental liquids, this can prove a strength as they are well-poised to establish universal trends applicable to a wide range of molecules. NEMD simulations of sheared model bulk liquids since the 1980s have revealed that an initial ambient liquid state typically transforms at steady-state into a partially ordered or crystalline arrangement in coexistence with a more amorphous liquid-like region [19–21]. A confined compressed liquid exhibits nonaffine flow in which the crystal-like and amorphous regions have different average shear rates, which in extreme cases may be referred to as "shear localization" or "banding." Depending on the applied conditions, it has been found that the nominal Couette shear velocity profile can localize into narrow bands either at the wall, where there is "slip," while the central region acts largely as a plug (plug-slip) in the middle of the gap. Alternatively, solidification of the liquid can occur at the walls and the shearing take place in the middle of the gap, which is referred to as "central

*c.gattinoni@imperial.ac.uk
†d.heyes@imperial.ac.uk
‡chris.lorenz@kcl.ac.uk
§d.dini@imperial.ac.uk

localization" in our previous publication [22]. Shear banding has been observed many times in experiments and NEMD simulations for a wide range of real and model particulate materials, such as glasses [23–25], colloids [26–29], pastes [30], and granular systems [31], and one might tentatively suggest that it is an inherent rheological feature of densely packed condensed matter in confinement. Shear banding is also seen to arise in bulk systems but only for liquids that are strongly thixotropic in nature, such as flocculated colloidal liquids [32,33], which are often relatively dilute; in this case the mechanism is thought to rely on a stress maximum in the constitutive equation of state [34]. Butler and Harrowell first explored in depth the phenomenon of shear banding for coexisting strained crystal ordered and disordered phases [20,21], whose basis it was discovered goes beyond "classical" mean-field and hydrodynamic theories of wall slip [35,36]. A viscosity kernel approach forms the basis of a more systematic explanation of the effects of density inhomogeneities [37]. The NEMD simulations to date have revealed the importance of the interaction potential between the wall atoms and the liquid molecules in governing the physical state of the confined liquid and its flow characteristics [4,38,39]. The influence of interface wettability on nanoscale flow has been investigated by NEMD [40], with nonwetting boundary conditions giving plug-like flow with a driving-pressure-dependent slip-length.

This work explores further a number of aspects of sheared confined liquids under pressure that were not addressed in Ref. [22] and sheds light on some important phenomena observed in confined lubrication. The low-shear-rate high-pressure solid regime in which stick-slip behavior is observed is investigated. The behavior of the traction coefficient in various parts of the nonequilibrium phase diagram is explored in more detail. The effects of partial to nonwetting of the liquid rheology and state are used to extend the scope of the nonequilibrium phase diagram to the nonwetting limit for the first time. The monatomic Lennard-Jones liquid used in Ref. [22] was employed, as well as a standard binary LJ mixture [41,42], designed to discourage crystallization. Temperature variations across the system and wall-based thermostatting strategies [36] are also discussed in this article.

II. METHODOLOGY

Systems of 40 000 atoms were simulated using the LAMMPS molecular dynamics package [43]. The atoms interact with the Lennard-Jones (LJ) potential, $U_{LJ}(r)$, which was modified to include a wetting parameter c:

$$U_{\mathrm{LJ}}(r) = 4\epsilon\left[\left(\frac{\sigma}{r}\right)^{12} - c\left(\frac{\sigma}{r}\right)^{6}\right].$$

In the above formula, r is the interatomic separation distance, and ϵ and σ are the Lennard-Jones coefficients. The interactions were truncated at a radius $r = 2.5\sigma$ and the parameters, ϵ and σ were assigned the values to describe argon, $\epsilon/k_B = 120$ K and $\sigma = 0.340$ nm, which are used throughout this article. The results are presented in a mixture of the usual Lennard-Jones units, and real units (for argon) to relate the MD results with experimental data. The c parameter was set to 1 for atoms of the same type, whereas for the interactions between the wall and confined liquid atoms, c was varied from $c = 0.1$ to $c = 1$ in order to study the effect of the extent of wetting by the liquid of the wall on the physical behavior of the confined liquid. The system was divided into three distinct sections, two walls of 18 432 atoms each and a liquid confined between the walls, as illustrated schematically in Fig. 1. The wall consisted of a face-centered cubic (100) lattice, which were assigned the LJ parameters $\sigma = 1$ and $\epsilon = 10$. The relatively large value of the parameter ϵ ensured that the wall remained solid under shear, at a density $\rho^* = 1.063$ LJ. This feature of the model will be shown below to be necessary to capture some of the key aspects of the tribological response of the system, which a wall of strongly tethered atoms would probably not be able to do.

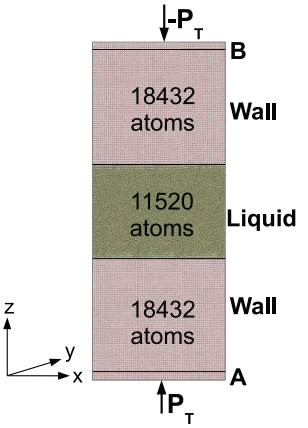

FIG. 1. (Color online) Schematic representation of the system.

Results have been obtained for two different types of liquid in between the solid walls. A monatomic system with $\epsilon = \sigma = 1$, as in Ref. [22], was used, and in addition simulations were carried out with the Kob-Barrat (KB) model binary mixture [41,42], which was designed originally to frustrate crystallization in a model supercooled liquid. In a mean-field sense, this enables us to explore the effects of molecular shape on the manifested tribology, as the KB mixture should behave more like a typical engine lubricant, rather than a traction fluid (the monatomic case). For the monatomic system, the LJ parameters were set to ϵ and σ, and the interactions between the atoms in the wall-liquid boundary region were obtained using the Lorentz-Berthelot mixing rules [44], whereas for the bidisperse system the values for these parameters were the specific ones given in Ref. [42]. The mass of all the atoms in the system was set to $m^* = 1$ in reduced units.

The simulations were performed with a target temperature of $T^* = 1$, through the use of a Langevin thermostat (LT) [45]. The most realistic way of achieving good temperature control in NEMD simulations has been the subject of numerous publications [36]. In the proposed system, only the walls were thermostatted, as it has been shown that thermostats applied to a confined sheared liquid add unphysical influences to the dynamics of the liquid itself [46,47]. The thermostat was applied only in the spanwise (y) direction to the wall atoms in order to avoid interfering with the external ("non-peculiar") velocities imposed on the system in the horizontal (x) and vertical (z) directions (the latter through the barostat). The damping or γ parameter of the LT was chosen as small as possible to maintain a steady-state system temperature with

minimal interference on the dynamics of the system, with $\gamma = 1$ (in reduced units) found to be the most suitable value.

A shear velocity gradient was imposed on the system by means of a constant velocity $\pm v_x$ applied to the boundary blocks A and B in the $\pm x$ directions. The normal pressure on the system was applied through two virtual "pistons," using the barostat method of Lupowski and van Swol [48,49] (to A and B in Fig. 1). The two layers of atoms at either end of the system in the vertical (z) direction have the same mass and initial velocity ($v^* = 0$). The barostat follows the equations

$$\begin{aligned} F_x &= F_y = 0, \\ F_z^A &= \frac{SP_T}{N_A} + \frac{\sum F_{\mathrm{LJ},A}}{N_A}, \\ F_z^B &= -\frac{SP_T}{N_B} + \frac{\sum F_{\mathrm{LJ},B}}{N_B}, \end{aligned} \tag{1}$$

where $F_{x,y,z}$ is the force applied at every time step in the x, y, and z directions, and it is nonzero solely in the normal (z) direction. S is the cross-sectional area of the system ($S \sim 348$ in reduced units), P_T is the target pressure, and N_A and N_B are the number of atoms in each of the two pistons (576 in this case). F_{LJ} is the average of the LJ forces for the atoms in the piston region. The averaging of the Lennard-Jones forces on these boundary pistons allowed us to treat A and B essentially as "blocks." The pressure was maintained on average constant in the z direction throughout the system by being applied to both ends of the system.

The timestep was $\Delta t^* = 0.001$ and typical simulation times were for $t^*_{\mathrm{eq}} = 1\,000$ for equilibration and $t^*_{\mathrm{pr}} = 3\,000$ for production. Equilibration was carried out with wall speed, $v_x = 0$, to ensure that the system had reached the desired temperature and pressure before applying the shearing action.

III. STRUCTURES UNDER SHEAR

The effects of wall velocity, pressure, and wetting were studied through a set of MD simulations covering representative values of these parameters. Relative wall velocities in the ranges $v^* = 0.012$–0.9 (corresponding to 2–150 m/s in standard units) and pressures $P^* = 2.37$–94.8 (corresponding to 100 MPa–4 GPa in standard units) were applied. The effect of the extent of wetting on the system behavior was analyzed for the monatomic LJ systems, whereas $c = 1$ (the maximum extent of wetting limit for this potential) was set for all of the binary mixture (BM) simulations. The results given below refer to the monatomic system unless otherwise stated.

A. Phase diagrams

For the monatomic system with high wettability ($0.5 < c < 1.0$), four main phases were observed [Fig. 2(a), top]: a liquid phase at low pressures, a solid phase at low velocities and high pressure, a plug-slip (PS) phase, and a central localization (CL) phase, in good agreement with Ref. [22]. In the case of low wettability ($c < 0.5$) the symmetry of the mixed phase is broken and instead of a central localization phase, asymmetric melting (AM) is observed instead [Fig. 2(a), bottom], which can occur at either wall. The third system studied (confined BM) does not show extensive ordering at any

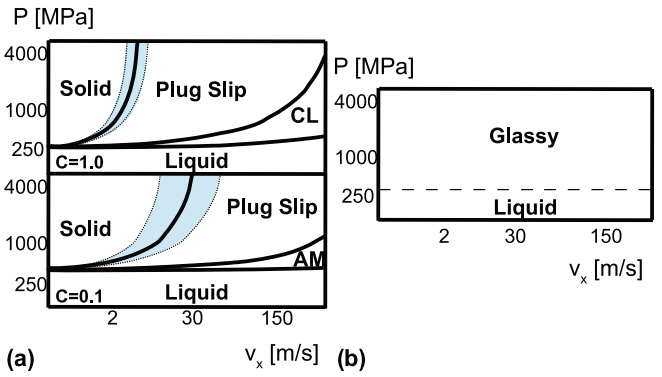

FIG. 2. (Color online) Phase diagram for (a) the monatomic and (b) the binary mixture systems. For the monatomic system (a), two phase diagrams are shown, one for $c = 1$ (top) and $c = 0.1$ (bottom). The main phases are labeled on the figure (CL stands for central localization and AM for asymmetric melting), and the solid black lines indicate the boundary between two phases. The shaded areas (blue online) highlight broad transition regions between coexisting phases.

pressure and velocity, maintaining a liquid or glassy behavior throughout the simulations, as shown in Fig. 2(b).

The equilibrium part of the phase diagram is shown in Fig. 2 on the ordinate (zero wall speed) axis. Only the liquid-solid part of the phase diagram is of relevance here because of the high pressures involved in the simulations. Previous molecular simulations have shown that walls induce layering of the liquid molecules, making the effective liquid part of the film smaller than the nominal thickness, which is what can be observed here. The liquid films used here are typically ~35 atomic layers thick. The evidence from previous simulation studies of even thinner confined LJ liquids indicates an insignificant change in the equilibrium liquid-solid coexistence pressure [4]. This was confirmed by our inspection of the zero wall speed states adopted by the confined films prepared by different routes in these simulations.

B. Liquid phase

The liquid phase is characterized by a linear velocity profile across the gap between the walls, as shown in Fig. 3(b) for the monatomic system and Fig. 4 for the binary mixture; this is the classical Couette flow solution for stick boundary conditions. The shading (color-coded online) in the diagram of the liquid-like monatomic system in Fig. 3(a) indicates the distance Δx the atoms have moved in the x direction from their initial position: $\Delta x = x(t_{\mathrm{final}}) - x(t_0)$. It confirms that the walls move at constant speed throughout the simulations while the confined liquid follows in a linear manner the moving walls, with the (light green online) area in the center being on average static. In the monatomic system, the liquid phase was observed at pressures up to 500 MPa for low values of the wetting parameter ($c = 0.1, 0.25$), whereas, for higher values of c, liquid-to-solid phase transitions were observed between 200 to 250 MPa. This can be explained by looking at the different density distribution [in Fig. 3 c)] in two 100 MPa systems. A higher value of c produces a greater accumulation of the liquid around the walls, giving a smaller liquid region

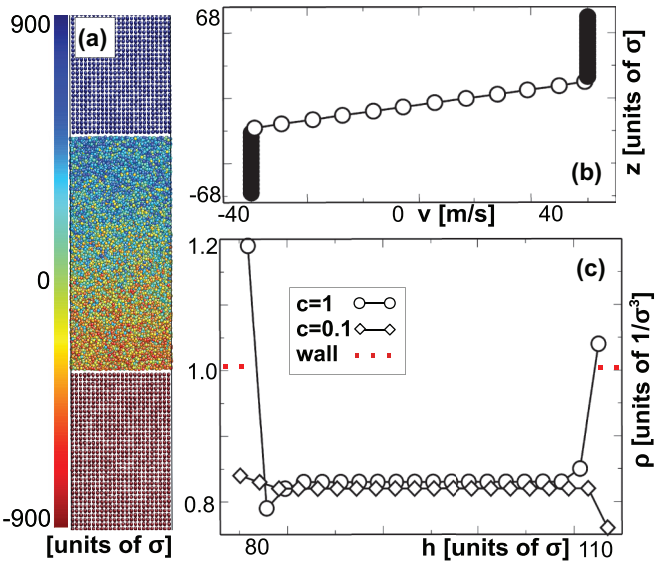

FIG. 3. (Color online) (a) Atom positions for the liquid-like phase, for a 100 MPa, 100 m/s, $c = 1$ system. The different colors indicate the displacement $\Delta x = x(t_{\text{final}}) - x(t_0)$ of the atoms at the end of the simulation, with respect to their original positions, with the distance unit being σ. (b) Corresponding velocity profile. (c) Density profile for 100 MPa, 100 m/s, c = 0.1, and c = 1.

thickness, whereas for a lower value of c the gap is $\sim 1\sigma$ wider and the overall density lower. It can thus be argued that the "critical density" (and wall separation) necessary for a phase transition is reached at different pressures for different values of c, with high values of c reaching it first.

In the BM system, the liquid phase is the only phase observed. The binary mixture components form distinct layers at the boundary (Fig. 4). The large more attractive liquid atoms (green online) with $\epsilon = 1$ and $\sigma = 1$ adsorb onto the wall first,

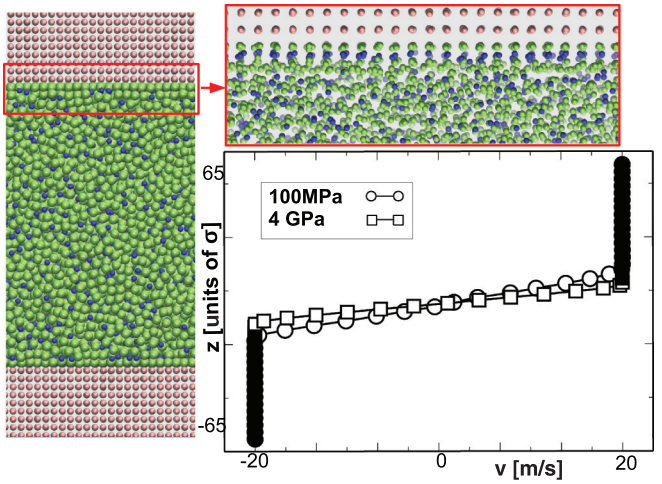

FIG. 4. (Color online) System formed by solid LJ walls and a confined binary mixture. The large atoms are green and the smaller ones are blue online. Alignment of these molecules in distinct layers at the boundary can be seen. The right-hand frame shows velocity profiles (at a wall speed of 20 m/s) for the system at pressures of 100 MPa and 4 GPa.

followed by a layer of the atoms with $\epsilon = 0.5$ and $\sigma = 0.88$ (blue online).

C. Solid phase

The solid phase is observed at high pressures (500 MPa to 4 GPa) and low velocities (2 m/s) and it is characterized by slipping predominantly at just one of the two walls [see Fig. 5(a)]. In this nonequilibrium phase, the structure is crystalline throughout the system and the atoms are perfectly aligned at the boundaries. Figure 5(b) shows the time evolution of the instantaneous value of the traction coefficient μ, which, throughout this work, was calculated as the ratio of shear $\sigma_{\parallel}$ divided by normal stress $\sigma_{\perp}$ according to the formula $\mu = \langle \sigma_{\parallel} \rangle / \langle \sigma_{\perp} \rangle$, where the angular brackets indicate time averages.

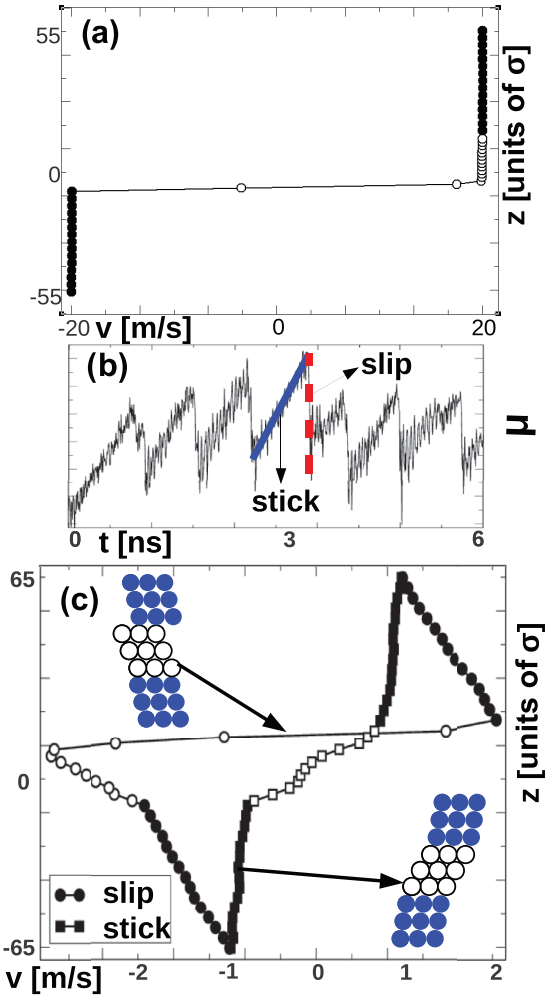

FIG. 5. (Color online) (a) Velocity profile of the system with a solid confined phase ($P = 4$ GPa, $v = 2$ m/s, $c = 1$). Closed symbols are used for the velocity of the wall atoms, open symbols for the velocity of the confined system. (b) Traction coefficient μ showing a series of "peaks" indicating the stick-slip behavior of the system. In the highlighted peak, the (blue online) solid line shows the "stick" behavior, the (red online) dashed line shows slip. (c) Velocity profile for the system during the stick-slip cycle highlighted in panel (b). The open symbols represent the confined system and the closed symbols are for the walls. The diagrams show the system configuration as the traction increases and decreases.

Stick-slip behavior, characterized by a cyclic pattern of peaks and troughs in the time evolution of μ, is evident. Build-up ("stick") and decrease ("slip") of the traction coefficient μ within one cycle are highlighted in Fig. 5(b) by a (blue online) solid line and a (red online) dashed line, respectively. The periodicity of the peaks is roughly equal to the average time it takes the shear strain at the boundary wall to move through one lattice spacing (of length $\sim 0.78\,\sigma$). In order to provide an insight into the system evolution in stick-slip conditions, velocity profiles calculated as time averages during the "stick" or "slip" part of the dynamics have been extracted and are shown in Fig. 5(c), together with schematics of the system configuration. In the "stick" velocity profile [o symbols in Fig. 5(c)], the velocities were averaged over the timesteps where the system shows an increase in the traction coefficient μ [bold solid blue line in Fig. 5(b)]; in the "slip" velocity profile [square symbols in Fig. 5(c)] the velocities were averaged over the timesteps where the system shows a decrease in the traction coefficient [bold red dashed line in Fig. 5(b)]. The system is seen to "stretch" in the build-up part of the cycle ["stick" in Fig. 5(c)], principally in the confined part but also partially in the walls, as represented in the schematics in Fig. 5(c). When it "fails" at one of the boundaries ["slip" in Fig. 5(c)] the two blocks accelerate in opposite directions and the wall-confined solid block advances by a single atomic step with respect to the other wall [see the schematic in Fig. 5(c)]. Significant deformation (~2–4%) of the solid wall is measured during this part of the cycle, which would not be captured if the wall atoms were strongly tethered. While a high degree of wall deformation might not be realistic to reproduce the behavior of hard materials, the ϵ and σ parameters in the Lennard-Jones potential can be tailored to reproduce the stiffness of real-life hard materials [9] or softer coatings [50], thus eliminating the need of tethering.

D. Plug-slip phase

The plug-slip phase presents slip at both boundaries and the amorphous central region acts as a plug, at zero velocity, while a small amount of melting is observed at the wall-liquid boundary (see Fig. 6). This phase occurs at higher velocities than the solid phase, as the shear stress needs to build up sufficiently to overcome the energy barriers linking the central region atoms to the walls. The PS phase is observed for all values of the wetting parameter, c. It exhibits a characteristic overshoot in the traction coefficient with time, which does not occur in other phases. The traction coefficient at short times is higher than its long-time limiting value because the boundary layer melts during the simulation and this causes μ to decrease until a steady state is reached and the traction coefficient plateaus to a lower average value. The shaded areas in Fig. 2 represent regions of velocity and pressure where a mixed-solid and plug-slip phase is observed, i.e., where the system is sufficiently strained for the slip to happen at both walls over a number of time steps.

E. Mixed phases

Two different mixed-phase cases are observed. Figure 7 (left frame) shows that for values of $0.5 < c < 1.0$, a CL phase

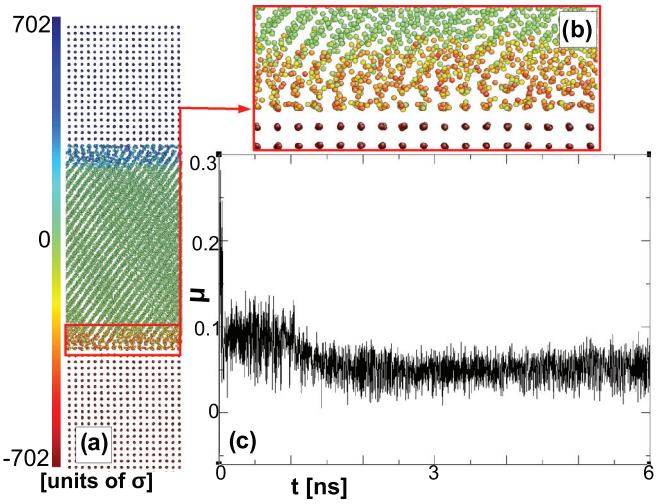

FIG. 6. (Color online) (a) Plug-slip configuration, after ca. ~ 7 ps of MD from the start of the production phase of the simulation, for $P = 1$ GPa, $v = 100$ m/s, and $c = 1$. The light coloring (light green online) of the central section of the system in the left frame shows that it has not moved with respect to its original position. (b) Close-up of the boundary layer. The confined atoms close to the ordered wall boundary (yellow/orange online) show more disorder and higher movement from their original position than those further away from the wall (light green online). (c) Traction coefficient for the whole duration of the simulation.

is seen, in which the confined material is mostly solid with a melted layer, whose thickness increases with the shear velocity, in the center and aligned parallel to the walls. This phase occurs at $P = 500$ MPa and at velocities greater than 40 m/s, and for $P = 1$ GPa and velocities greater than 100 m/s. For low values of c, the symmetry of the system breaks and the mixed phase observed consists of melting at one of the boundaries only (see Fig. 7, right frame). This phase is found only for $P = 500$ MPa and $v = 80$ m/s upwards and the thickness of the molten layer

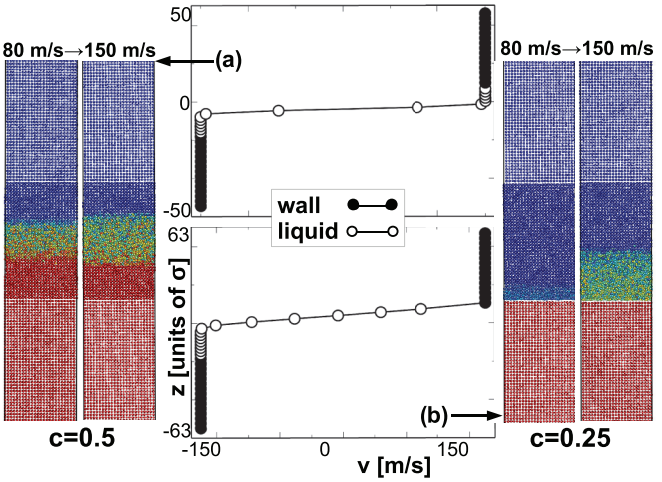

FIG. 7. (Color online) Instantaneous configuration and velocity profiles for a system exhibiting (a) central localization (left diagram, for $c = 0.5$ and $P = 500$ Mpa) and (b) asymmetric melting (right diagram, $c = 0.25$ and $P = 500$ Mpa). The melted areas are shown in a lighter colour (green online) at the centre of the CL system and at the bottom boundary of the AM system.

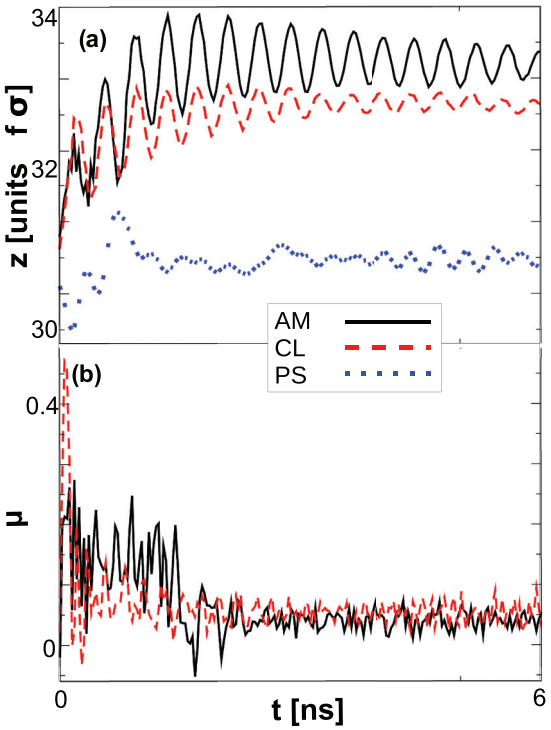

FIG. 8. (Color online) Time evolution of (a) Wall separation h for a PS, CL, and AM system and (b) traction coefficient μ for a CL, and AM system at 500 Mpa, for the first 6 ns of a simulation.

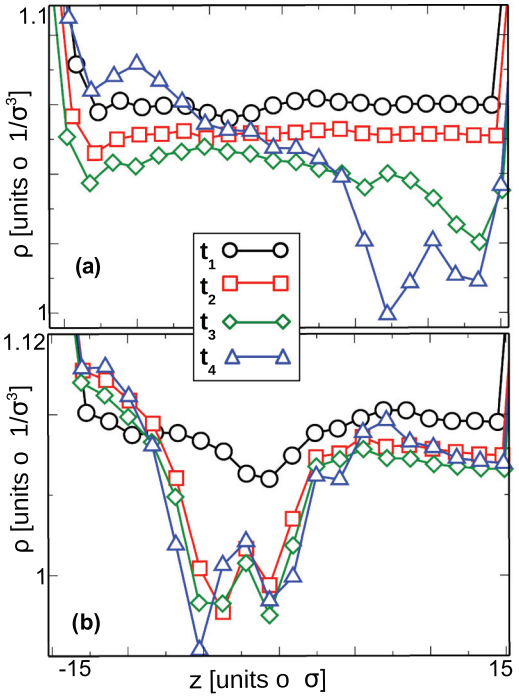

FIG. 9. (Color online) Number density evolution as a function of time from the start of the simulation in the confined section of the system, for (a) a PS-to-AM transition and (b) a PS-to-CL transition.

grows with the shear velocity. It is observed that the film thickness, h, increases significantly in these phases ($\sim 2\,\sigma$s more than in the PS phase), as shown in Fig. 8(a), and it can be argued that the phase transitions are triggered by this system dilation. In order to verify this hypothesis, two simulations were carried out under the same conditions of velocity and pressure ($P = 500$ MPa and $v = 80$ m/s) for the $c = 0.5$ system shown in Fig. 7; one simulation with the barostat turned on, the other having fixed wall separation (leaving no space for expansion of the system in the z direction). In the simulation where the wall was allowed to relax vertically, the PS-to-CL transition took place, while for fixed wall separation the CL phase transition was not seen. The time evolution of the traction coefficient [Fig. 8(b)] and of the density profile (Fig. 9) give further insight into the formation of these two phases. In the case of the CL phase, the wall separation h [Fig. 8(a)] dilates to $h \sim 32.5\,\sigma$, a variation corresponding broadly to the size of a single atom, a phenomenon which has been observed elsewhere [50–52]. The traction coefficient μ grows in the first ~5 LJ units of the simulation evolution [Fig. 8(b)] before collapsing as the system starts shearing in the middle. As the wall separation increases, the confined material becomes less cohesive and preferentially shears in the middle of the confined film. Figure 9(b) confirms that the CL system had melted in the center of the confined system after 10 LJ time units, in contrast to the AM system, which started to melt only after 70 LJ units [Fig. 9(a)]. A close inspection of the AM system evolution shows that, starting from the equilibrium configuration at $P = 500$ MPa, with all atoms in the system aligned in FCC configuration, the system initially undergoes a transition to a PS phase, which proceeds with a small amount of stick slip [Fig. 8(b)] and with minimal melting [1–2 atomic layers, Fig. 9(b)] at both boundaries and steady growth of the wall separation. When a density $\rho \sim 1.05$ is reached, melting deepens at one of the two boundaries giving rise to the asymmetry in the system.

IV. TRACTION

The physical state of the lubricant in elastohydrodynamic lubrication in concentrated contacts is still largely unresolved, owing to experimental difficulties in probing the contact zone under operating conditions. Traction coefficients are used in tribology as a measure of the sliding property of a material and they are preferred to the friction force, which is directly measured in experiments as they do not depend on the total surface area and on the load, thus making measurements at different shear rates easy to compare. For high-pressure lubricants, the literature has focused mainly on two types of traction curves: Ree-Eyring or Newtonian-to-plastic flow models. In the Ree-Eyring model, the traction coefficient increases with shear rate with an ever-decreasing slope, in the Newtonian-to-plastic-flow model, there is a relatively sharp transition from a constant (Newtonian) to zero slope (plastic flow) at a critical shear rate (wall speed) [53]. An additional complication that casts doubt on both of these models was given by Bair and coworkers who provided experimental evidence of shear localization in the film at an angle to the walls [54], later with theoretical support [55]. This shear localization does occur in our simulations, although not in exactly the same form. This observation confirms the potential inappropriateness of these bulk rheological

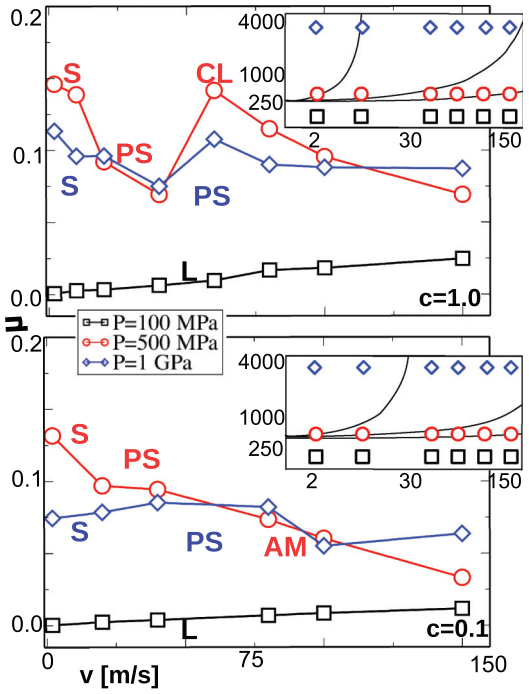

FIG. 10. (Color online) Time-averaged traction coefficients for $c = 1$ and $c = 0.1$ and different pressures in the monatomic LJ system. The pressure and wall speeds used are indicated on the phase diagram in the insets.

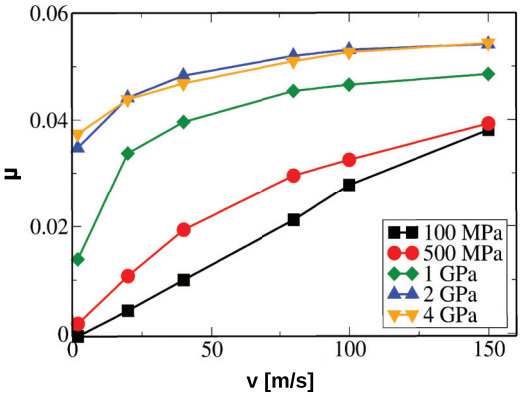

FIG. 11. (Color online) Traction coefficient for all pressures and velocities for a binary mixture.

constitutive equations in at least some of the flow and load conditions encountered in experiment (e.g., at relatively high pressure).

Figure 10 presents the wall-speed dependence of the traction coefficient μ as a function of pressure for the monatomic systems with $c = 1.0$ (top frame) and $c = 0.1$ (lower frame). The trends evident on the figures are statistically significant: when reproducing the simulations with different starting configurations and same parameters, the maximum error found between simulations was $\delta\mu = 0.004$ for $c = 0.1$ and $\delta\mu = 0.02$ for $c = 1$. For the same values of pressure and velocity, the traction coefficient is lower for $c = 0.1$ than for $c = 1$. A lower attractive force between the atoms on either side of the boundary diminishes the shear stress at the boundary. In the case of a liquid-like system (100 MPa, black line in Fig. 10), where no phase transition occurs with increasing wall speed, the traction coefficient increases linearly with v_x, as expected. At very high pressures (4 GPa in Fig. 10) the evolution of the traction coefficient μ with respect to the velocity v_x can be considered approximately flat ($\overline{\mu}_{c=1} = 0.0942 \pm 0.011$, $\overline{\mu}_{c=0.1} = 0.073 \pm 0.011$), within the simulation error. Instead, different phases can be recognized in the traction coefficient plot at intermediate pressures (500 MPa in Fig. 10). High traction is found for the solid or semisolid phases, where at low velocities the predominant force is the wall-solid adhesion. The melted layer at both wall-solid boundaries produces a lower traction coefficient, which is found in both wetting and nonwetting case. In the nonwetting $c = 0.1$ case, the value of μ decreases steadily as the velocity increases for the AM phase, which is consistent with the fact that the melted volume grows steadily. For the $c = 1$ case, another high-traction region is identified at the onset of the CL phase, then decreasing for higher values of v_x, with the increase in size of the melted layer. It has been observed that the maximum traction for all the systems is obtained for 500 MPa at low velocities, consistent with the results obtained in Ref. [22] and with an increase in the shear modulus at high pressures.

In the case of the confined binary mixture, the traction coefficient behavior is illustrated in Fig. 11. The linear relationship of the traction coefficient μ with sliding velocity, already seen in the monatomic case for low pressures, holds only for pressures in the region of 100 to 200 MPa. In all other cases, the curves gradually converge toward a plateau with sliding speed typical of compressed liquids bordering on highly nonlinear rheological "glassy" behavior. This is qualitatively what would be expected for the Ree-Eyring fluid [53].

V. TEMPERATURE PROFILES

Temperature profiles have been extracted for all the simulations and Fig. 12 shows those for all pressures at 100 m/s, a velocity where all phases are observed for $c = 0.1$ and $c = 1$. The average velocity in the x direction, which is induced by the applied shear velocity to the boundaries, has been subtracted from the particle velocities before calculating the temperature from the kinetic energy. The maximum temperature recorded in the system was $T^* \sim 1.5$, observed at high pressure and velocities, decreasing rapidly at the wall-liquid interface, showing the effectiveness of the thermostat in dissipating the heat through the wall atoms. Distinct patterns have been observed corresponding to each phase, showing higher temperatures in denser (e.g., higher pressure) or more disordered (e.g., melted) sections of the confined system. In the liquid phase at low pressure the profile appears approximately flat with no jump at the wall boundary. In the PS phase, a jump at the boundary is evident: the solid-like "plug" area between the walls has an approximately constant temperature, rising toward the melted walls, and it is lower in the walls themselves. In the CL phase, the highest temperature is found in the liquid center of the system, growing linearly and with no discontinuity at the wall boundary. Finally, the AM phase shows an asymmetric temperature profile, with a higher temperature close to the bottom wall, where the melting is

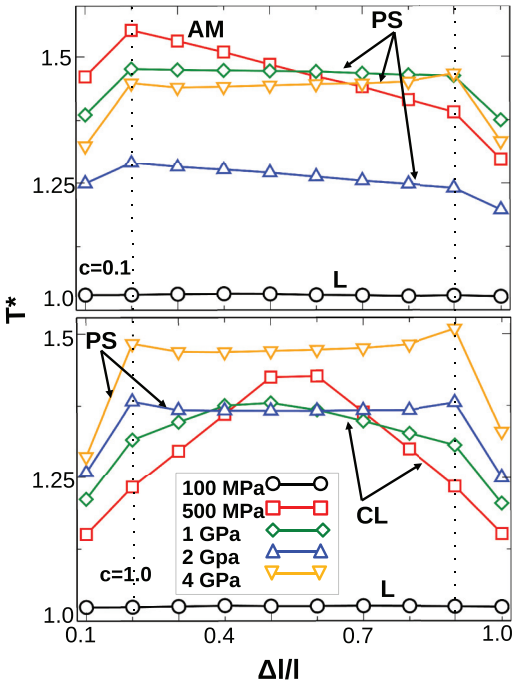

FIG. 12. (Color online) Temperature profiles for the central part of the system and a section of the walls for $c = 1$ and $c = 0.1$ for all pressures at 100 m/s. The boundary between walls and confined system is indicated by vertical dashed lines, with the bottom wall being on the left and the top wall on the right. The temperature on the vertical axis is in reduced units. On the horizontal axis, l is the height of the system considered in the computation of the temperature and Δl is the length of each "slice" in which the system has been divided.

taking place. In the binary mixture system, the temperature profiles show a parabolic shape in the unthermostatted central region, which can be compared with the prediction of Fourier's law of heat conduction [56]. Following the analysis in Ref. [22], the temperature in the liquid $T_L(z)$ can be written as:

$$T_L(z) = -\frac{P_{xy}\dot{\gamma}z^2}{2\lambda} + a, \quad 0 \leqslant z \leqslant z_1, \tag{2}$$

where P_{xy} is the shear stress, z is defined as the distance from the center of the system, $\dot{\gamma}$ is the shear rate, λ is the thermal conductivity of the region, and a is an integration constant. The value of a was obtained by comparing the temperature of the liquid and of the solid boundary at z_1. The temperature of the solid boundary is assumed to be a constant T_c across z as the wall is thermostatted, leading to

$$a = T_c + \frac{P_{xy}\dot{\gamma}z_1^2}{2\lambda}. \tag{3}$$

The value of λ was obtained through a least-squares fit, giving the curves in Fig. 13. Good agreement is obtained between the simulation data and the fitted curves, showing that the expected temperature profile in the confined liquid for this system can be approximated by a parabola where the curvature is determined through the macroscopic shear stress and shear rate condition, $(P_{xy}\dot{\gamma})/(2\lambda)$. The values of the thermal conductivity are found to increase with the system pressure (see the caption of Fig. 13) and therefore with stronger interactions between the atoms.

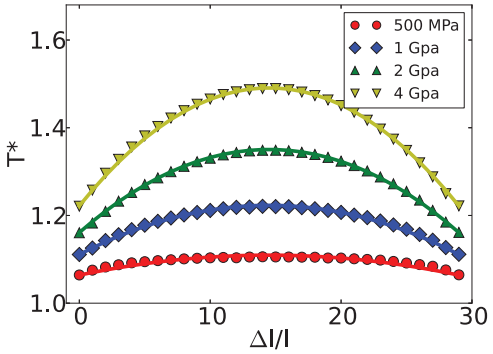

FIG. 13. (Color online) Temperature profile for all pressures at 100 m/s for the binary mixture. The temperature is shown on the vertical axis and the z coordinate on the horizontal axis. LJ units have been used. The calculation has been performed for the confined liquid only. The symbols represent the simulated data, whereas the solid line represents the theoretical fit of Eq. (2). The thermal conductivities found by fitting the simulation data to Eq. (2) are: $\lambda_{500\,\mathrm{MPa}} = 37.38$, $\lambda_{1\,\mathrm{GPa}} = 42.74$, $\lambda_{2\,\mathrm{GPa}} = 58.37$, $\lambda_{4\,\mathrm{GPa}} = 79.63$, in reduced units.

Poiseuille flow NEMD studies [57] have demonstrated that including strain rate coupling in the theoretical description of the temperature profile improves the fit to the simulation data. Although this extra term is zero for ideal Couette flow, the strain rate localization observed here for the monatomic NEMD simulations systems at high pressure indicate that it should be included in any theoretical treatment. This might explain, at least in part, why the monatomic NEMD temperature profiles produced here are generally far from quadratic.

VI. VISCOSITY

In the monatomic system, the liquid (apparent) viscosity, η, for pressure $P = 100$ MPa was calculated as the slope of the wall shear stress, $\sigma_\parallel$, as a function of the apparent shear rate, $\dot{\gamma}$ following Couette flow theory. Figure 14(a) shows that η increases with c at 100 MPa as expected, as the interaction between liquid and wall particle increases. This derived quantity is an apparent viscosity as it is influenced by the contact of the liquid to the boundary walls, rather than being an intrinsic property of the bulk liquid itself, which is what experimentalists measure. The values shown, converted to real units, are $\sim$200 μPa s, in good agreement with values for real liquid argon at $T^* = 1$ (120 K in real units) [58]. In the case of the binary mixtures, Figs. 14(b) and 14(c) reveal that, as for the traction coefficient μ, at pressures higher that 500 MPa the viscosity is no longer Newtonian, but the curves converge toward a plateau. For the Newtonian case of $P = 100$ MPa, the viscosity can be calculated from the slope of the graph in Fig. 14, which gives a value of $\eta = 291.8$ μPa s.

VII. CONCLUSIONS

In this work the study of confined sheared model liquids under pressure commenced in Ref. [22] has been continued and significantly extended with much larger system sizes, and a more extensive exploration of the parameter space and physical

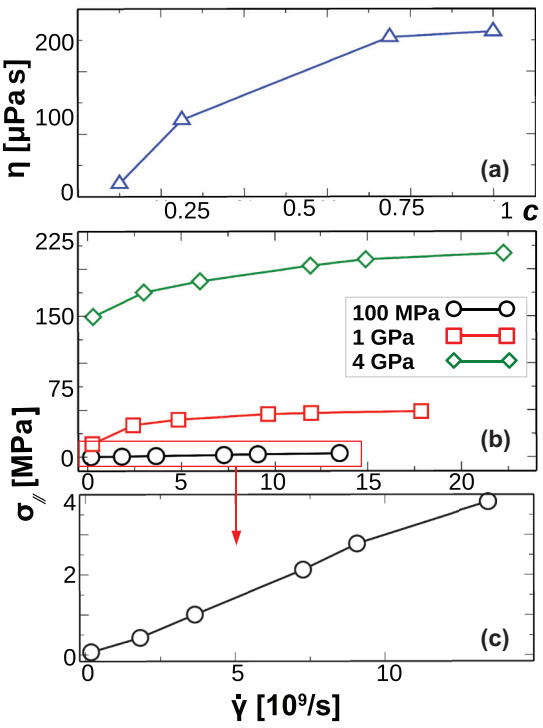

FIG. 14. (Color online) (a) Viscosity as a function of the wetting parameter c, for simulations at $P = 100$ MPa for a monatomic LJ confined liquid. (b) Shear stress/shear rate diagram for $P = 100$ MPa, 1 GPa, 4 GPa, and all velocities, for a confined binary mixture. (c) Close up of the shear/shear rate graph b for $P = 100$ for a binary mixture.

effects. A theme that emerges from the present study is the importance of the wall-liquid boundary conditions in determining the tribological behavior of confined liquids under shear at high pressure. In this study we include variable wettability of the solid wall by the liquid, and whether the walls are constrained to be at a fixed separation or adjusted to maintain a prescribed normal pressure.

Considering first the monatomic model liquid, several aspects of the previous model have been studied in more detail. The first is the evolution of the solid phase at low wall speed and moderately high pressure. The microscopic mechanism of the so-called "stick-slip" phenomenon is uncovered in new detail, which has been widely investigated for experimental and model confined liquids. At moderately high pressure, the stick part of the cycle is accompanied by a large deformation of the solid wall next to the entrained liquid (in fact this is "true" stick). The slip part of the cycle involves a rapid relaxation of the strained solid and slip at the wall. The velocity of the wall next to the confined liquid suddenly increases as this region catches up with the imposed displacement of the two outer wall regions. Although speculation in the past has suggested that wall deformation can play a role in high-pressure tribology, this is the first supportive evidence to come directly from NEMD that this can be the case. Such an effect would probably not have been seen with wall atoms strongly tethered to a sublattice.

The nonequilibrium phase diagram is strongly influenced by whether the film thickness or external pressure is held fixed during the simulation. At constant thickness, the central region shear banding can be suppressed in favor of shear banding or slip at the wall.

The effect of varying the wetting parameter, c, was observed to have a significant qualitative effect on the phase and traction coefficient behavior. For $c \to 0$, the confined liquid hardly wets the wall, while the maximum wetting achievable using the Lennard-Jones potential is when $c = 1$. More complete phase diagrams are present for both $c = 0.1$ and $c = 1$, with more data generated for in-between values of c. It has been established that in the poor wetting limit for sliding speeds (above what we call the "plug-slip" (PS) state for the good wetting state), the extensive shear-melted liquid region forms at the boundary with the wall as an extension of the boundary slip region at lower values of wall speed. The thickness of the liquid-like region increases with sliding speed, with the shear stress in the confined material never exceeding its bulk yield stress value. In contrast, in the largest extent of wetting limit, the liquid state beyond the PS state is initiated in the *center* of the gap, which continues to grow in width with increasing wall speed. Therefore, we conclude that the interaction between the wall and the confined liquid influences qualitatively the tribological behavior of the whole system, rather than just in the immediate vicinity of the boundary, and especially in the way the system responds to applied pressure. The implication for more complex lubricants is that wettability can yield significantly different results in the dynamics of the *whole* confined system under shear.

Simulations of a binary mixture of Lennard-Jones atoms modeled by nonequilibrium molecular dynamics is another new feature of this work. It has been observed that a single component or monoatomic liquid has a tendency to crystallize in the FCC geometry, which is suppressed in the binary mixture under consideration [42]. Simulations performed under the same conditions of temperature, pressure, and velocity have shown that the two systems differ remarkably in their response to applied shear straining. The monoatomic system presents a variety of phase transitions that depend on its favorable tendency to crystallize, whereas the binary mixture system does not form ordered structures and shows instead a more traditional liquid-like response and glassy behavior at high pressure with attendant nonlinear response with velocity, indicative of significant shear thinning. The monatomic system is probably closer to a traction fluid composed of quasispherical molecules, whereas the binary mixture is nearer in physical response to the oligomeric molecules found in typical lubricants. Detailed studies of such large molecules are necessary in order to establish the role that molecular structure and complex molecular interactions can have on the overall dynamics and tribology of the confined system under shear and pressure. The present study provides a preliminary insight into what might be expected.

ACKNOWLEDGMENTS

The authors acknowledge the financial support received from the Engineering and Physical Sciences Research Council (EPSRC) via Platform Grant No. EP/G026114/1.

[1] R. Buzio, C. Boragno, and U. Valbusa, J. Chem. Phys. **125**, 094708 (2006).
[2] P. Jop, Y. Forterre, and O. Pouliquen, Nature **441**, 727 (2006).
[3] L. Bertocchi, D. Dini, M. Giacopini, M. T. Fowell, and A. Baldini, Tribol. Int. **67**, 61 (2013).
[4] H. Kanda, M. Miyahara, and K. Higashitani, J. Chem. Phys. **120**, 6173 (2004).
[5] A. Vishnyakov and A. V. Neimark, J. Chem. Phys. **118**, 7585 (2003).
[6] T. Fehr and H. Lowen, Phys. Rev. E **52**, 4016 (1995).
[7] M. Tsige and S. S. Patnaik, Chem. Phys. Lett. **457**, 357 (2008).
[8] A. Jabbarzadeh, P. Harrowell, and R. I. Tanner, Phys. Rev. Lett. **94**, 126103 (2005).
[9] H. Docherty and P. T. Cummings, Soft Matt. **6**, 1640 (2010).
[10] H. Yoshizawa and J. Israelachvili, J. Phys. Chem. **97**, 11300 (1993).
[11] H. W. Hu, G. A. Carson, and S. Granick, Phys. Rev. Lett. **66**, 2758 (1991).
[12] L. Bureau, Phys. Rev. Lett. **104**, 218302 (2010).
[13] S. Granick, Science **253**, 1374 (1991).
[14] C. Drummond and J. Israelachvili, Phys. Rev. E **63**, 041506 (2001).
[15] P. A. Thompson and M. O. Robbins, Science **250**, 792 (1990).
[16] S. T. Cui, P. T. Cummings, and H. D. Cochran, J. Chem. Phys. **114**, 7189 (2001).
[17] A. Jabbarzadeh, P. Harrowell, and R. I. Tanner, J. Chem. Phys. **125**, 034703 (2006).
[18] E. Kumacheva and J. Klein, J. Chem. Phys. **108**, 7010 (1998).
[19] D. M. Heyes, J. Chem. Soc.-Faraday Trans. II **82**, 1365 (1986).
[20] S. Butler and P. Harrowell, J. Chem. Phys. **118**, 4115 (2003).
[21] S. Butler and P. Harrowell, Phys. Rev. E **67**, 051503 (2003).
[22] D. M. Heyes, E. R. Smith, D. Dini, H. A. Spikes, and T. A. Zaki, J. Chem. Phys. **136**, 134705 (2012).
[23] Y. F. Shi and M. L. Falk, Phys. Rev. B **73**, 214201 (2006).
[24] P. Chaudhuri, L. Berthier, and L. Bocquet, Phys. Rev. E **85**, 021503 (2012).
[25] F. Varnik, L. Bocquet, J. L. Barrat, and L. Berthier, Phys. Rev. Lett. **90**, 095702 (2003).
[26] K. Yeo and M. R. Maxey, Phys. Rev. E **81**, 051502 (2010).
[27] W. M. Holmes, P. T. Callaghan, D. Vlassopoulos, and J. Roovers, J. Rheol. **48**, 1085 (2004).
[28] J. R. Seth, C. Locatelli-Champagne, F. Monti, R. T. Bonnecaze, and M. Cloitre, Soft Matt. **8**, 140 (2012).
[29] P. Coussot, J. S. Raynaud, F. Bertrand, P. Moucheront, J. P. Guilbaud, H. T. Huynh, S. Jarny, and D. Lesueur, Phys. Rev. Lett. **88**, 218301 (2002).
[30] V. Bertola, F. Bertrand, H. Tabuteau, D. Bonn, and P. Coussot, J. Rheol. **47**, 1211 (2003).
[31] P. Schall and M. van Hecke, Ann. Rev. Fluid Mech. **42**, 67 (2010).
[32] P. C. F. Moller, S. Rodts, M. A. J. Michels, and Daniel Bonn, Phys. Rev. E **77**, 041507 (2008).
[33] T. Divoux, D. Tamarii, C. Barentin, and S. Manneville, Phys. Rev. Lett. **104**, 208301 (2010).
[34] P. C. F. Moller, J. Mewis, and D. Bonn, Soft Matt. **2**, 274 (2006).
[35] E. Lauga, M. P. Brenner, and H. A. Stone, *Handbook of Experimental Fluid Dynamics*, edited by J. Foss, C. Tropea, and A. Yarin (Springer, New York, 2005).
[36] H. Berro, N. Fillot, P. Vergne, T. Tokumasu, T. Ohara, and G. Kikugawa, J. Chem. Phys. **135**, 134708 (2011).
[37] P. J. Cadusch, B. D. Todd, J. Zhang, and P. J. Daivis, J. Phys. A **41**, 035501 (2008).
[38] C. Liu and Z. Li, Phys. Rev. E **80**, 036302 (2009).
[39] C. Liu and Z. Li, J. Chem. Phys. **132**, 024507 (2010).
[40] G. Nagayama and P. Cheng, Int. J. Heat Mass Trans. **47**, 501 (2004).
[41] W. Kob and H. C. Andersen, Phys. Rev. Lett. **73**, 1376 (1994).
[42] W. Kob and J. L. Barrat, Eur. Phys. J. B **13**, 319 (2000).
[43] S. Plimpton, J. Comp. Phys. **117**, 1 (1995).
[44] M. P. Allen and D. J. Tildesley, *Computer Simulation of Liquids* (Clarendon, Oxford, 1987).
[45] T. Schneider and E. Stoll, Phys. Rev. B **17**, 1302 (1978).
[46] S. Bernardi, B. D. Todd, and D. J. Searles, J. Chem. Phys. **132**, 244706 (2010).
[47] D. J. Evans and G. P. Morriss, Phys. Rev. Lett. **56**, 2172 (1986).
[48] M. Lupkowski and F. Vanswol, J. Chem. Phys. **93**, 737 (1990).
[49] M. Lupkowski and F. Vanswol, J. Chem. Phys. **95**, 1995 (1991).
[50] C. D. Lorenz, J. Matthew D. Lane, M. Chandross, M. J. Stevens, and G. S. Grest, Langmuir **25**, 4535 (2009).
[51] L. Ramin and A. Jabbarzadeh, Langmuir **28**, 4102 (2012).
[52] A. Dhinojwala, S. C. Bae, and S. Granick, Tribol. Lett. **9**, 55 (2000).
[53] S. Bair and W. O. Winer, J. Trib.-Trans. ASME **114**, 1 (1992).
[54] S. Bair, F. Qureshi, and W. O. Winer, J. Trib.-Trans. ASME **115**, 507 (1993).
[55] S. Bair and C. McCabe, Trib. Int. **37**, 783 (2004).
[56] B.-Y. Cao, J. Chem. Phys. **129**, 074106 (2008).
[57] B. D. Todd and D. J. Evans, Phys. Rev. E **55**, 2800 (1997).
[58] B. A. Younglove and H. J. M. Hanley, J. Phys. Chem. Ref. Data **15**, 1323 (1986).